Contact angle of ethanol, water, and their mixtures on stainless steel surfaces in dense carbon dioxide

Aymeric Fabien, Guillaume Lefebvre, Elisabeth Badens, Brice Calvignac, Damien Chaudanson, Alain Ranguis, Christelle Crampon

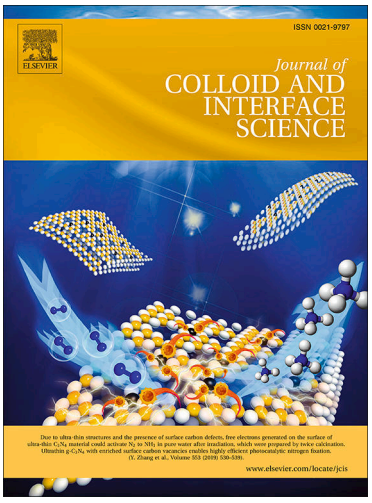

Contact angle of ethanol, water, and their mixtures on stainless steel surfaces in dense carbon dioxide

Aymeric Fabien, Guillaume Lefebvre, Elisabeth Badens, Brice Calvignac, Damien Chaudanson, Alain Ranguis, Christelle Crampon

PII: S0021-9797(23)02096-9
DOI: https://doi.org/10.1016/j.jcis.2023.10.163
Reference: YJCIS 33488

To appear in: *Journal of Colloid and Interface Science*

Received Date: 18 July 2023
Revised Date: 25 October 2023
Accepted Date: 31 October 2023

Please cite this article as: A. Fabien, G. Lefebvre, E. Badens, B. Calvignac, D. Chaudanson, A. Ranguis, C. Crampon, Contact angle of ethanol, water, and their mixtures on stainless steel surfaces in dense carbon dioxide, *Journal of Colloid and Interface Science* (2023), doi: https://doi.org/10.1016/j.jcis.2023.10.163

Contact angle of ethanol, water, and their mixtures on stainless steel surfaces in dense carbon dioxide

Aymeric Fabien[a], Guillaume Lefebvre[b], Elisabeth Badens[a*], Brice Calvignac[b], Damien Chaudanson[c], Alain Ranguis[c], Christelle Crampon[a]

[a] **Aix Marseille Univ**, CNRS, Centrale Marseille, **M2P2**, Marseille, France

[b] **Univ Angers**, Inserm, CNRS, **MINT**, SFR ICAT, F-49000 Angers, France

[c] **Aix Marseille Univ**, CNRS, CINAM, Marseille, France

* *Corresponding author*

Abstract

Hypothesis

Contact angle can be a key parameter in chemical engineering. However, the development and the optimization of numerous processes using supercritical CO_2, considered as environmentally friendly, requires new measurements under dense CO_2 atmosphere. Besides, the influence of the roughness or the wetting regime on the contact angle is known at ambient conditions but remains to be discussed for systems under high pressure.

Experimental

Contact angle measurements of ethanol, water, and their mixtures, with ethanol mass fractions ranging from 0.25 to 0.75, on two stainless steels in saturated CO_2 at pressures ranging from 0.1 MPa to 15.1 MPa, and at 313 K and 333 K were carried out in a set-up improving mass transfer between the studied liquid and the continuous fluid phase. Stainless steel surfaces have been characterized by atomic force and scanning electron microscopies allowing the application of the Wenzel equation.

Findings

Ethanol wetted totally both stainless steels while contact angles of all other liquids were increased by the rise of pressure, with contact angles up to 128 ° for water at 15.1 MPa. Trapped bubbles were observed at the solid/liquid interface and the bubble formation is discussed. Furthermore, the potential influence of bubble presence on the wetting regime is prospected through the question: could the pressure rise modify the wetting regime?

Keywords: Contact angle measurement; sessile drop method; ethanol; water; ethanol-water mixtures; supercritical carbon dioxide; high pressure; stainless steel surface characterization; wetting regime

1. Introduction

Several studies on contact angle have been carried out for systems under atmospheric conditions, while measurements of contact angle under high-pressure conditions, especially in supercritical carbon dioxide ($scCO_2$) atmosphere, remain limited in the literature. Nonetheless, $scCO_2$ is nowadays considered in various industries (food, nutraceutical, pharmaceutical, material…) as an alternative to conventional processes using organic solvents. An increasing interest has been observed for it in the development of industrial processes more respectful for the operators, the consumers, and the environment. Indeed, supercritical fluids (SCF) have liquid-like densities, gas-like viscosities, and

diffusion coefficients higher than liquids, giving them valuable solvent properties and are also considered as green solvents. It is specifically the case of $scCO_2$ [1]. Hence, contact angles under high pressure and/or high temperature conditions are now under investigation as key parameters in several process designs since they bring a better understanding of transfer phenomena, for instance, in heat transfer studies in a "water pressurized reactor" (WPR) nuclear power plant [2], or in a mass transfer studies dealing with packing wettability in $scCO_2$ fractionation of liquid mixtures [3–8]. Besides, the influence of interfacial properties on flooding phenomena in counter-current column is given less attention in literature due to the lack of data, though they are suspected to play a key role in several studies [9–13]. Contact angles of water on stainless steel or silicon, in pressurized N_2 at high temperature [2,14], as well as contact angles of water [3–5], ethanol [5] or lipid mixtures [7,8] on stainless steel, polymeric surfaces or glass in $scCO_2$ medium have been carried out. However, the studied systems remain lacunary in comparison to the diversity of liquid mixtures treated by SCF processes [6], and further measurements are still needed to link interface science and chemical engineering applied to high-pressure systems.

Contact angle (θ) of a liquid droplet on a solid surface, in a gas or SCF atmosphere, is defined as the angle delimited by the tangent, starting from the triple contact point and along the drop shape; and the contact line between the liquid and the solid, as shown in Figure 1.

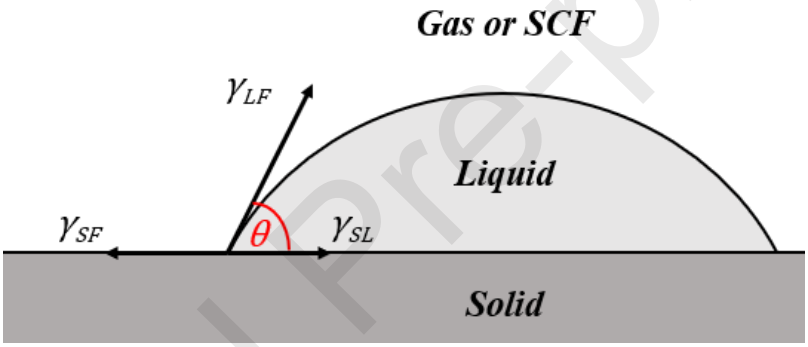

Figure 1 Schematic sessile drop at equilibrium following the Young approach with force balance at the triple contact point

The contact angle can be measured from photographs of a static liquid droplet deposited on a solid surface and by image processing, which is known as the sessile drop method. Its value is between 0 and 180° and is used to characterize the wettability of a liquid on a solid surface under given operating conditions. A contact angle lower than 90° indicates that the liquid wets well the solid, and a contact angle greater than 90° indicates a "bad wetting" of the system. Besides, if the liquid forms a film instead of a drop, with a contact angle close to zero, the wetting is said to be complete, total, or perfect. Otherwise, the wetting is said to be partial when the liquid forms a drop.

The contact angle depends on the nature of the continuous phase, gas or dense fluid, the liquid and the solid as well as operating pressure and temperature [14]. From a theoretical point of view, for a drop deposited on an ideal surface (perfectly smooth and homogeneous), the static contact angle at equilibrium, also called Young contact angle (θ_Y). It is described by the Young equation (Eq. (1)) which results from the force balance at the triple contact point [15,16], and where γ_{SF}, γ_{SL} and γ_{LF} are the solid/fluid, the solid/liquid and the liquid/fluid interfacial tensions, respectively.

$$\gamma_{SF} = \gamma_{SL} + \cos\theta_Y \cdot \gamma_{LF} \quad (1)$$

Further studies at atmospheric conditions also pointed out the influence of the surface roughness on the apparent contact angle, and the Wenzel equation (Eq. (2), presented in detail in section 2.3), can be used

to correct this effect if the system is supposed to be in the Wenzel state, i.e. if the wetting is homogeneous [17–20]. Also, the influence of the surface chemical heterogeneity was also investigated in the work of Cassie-Baxter [21] and the eponym equation (Eq. (6), presented in section 3.5) can be used to take this effect into account in the correction of the apparent contact angle if the system is in the Cassie-Baxter state, i.e. if the wetting is heterogeneous [17,19]. Gao and McCarthy [22] started a discussion about both representation of Wenzel and Cassie-Baxter indicating that the surface characteristics must be in accordance with the characteristics at the three phase line contact for the correct use of both Wenzel and Cassie-Baxter equations. Furthermore, the influence of an adsorption layer on wettability of the solid is also known [23–25], and has been pointed out in the literature for systems involving dense CO_2 [8,26]. Besides, the hysteresis observed for dynamic contact angle are also under investigation in current literature [17,19,20,27]. Nonetheless, these fundamental considerations of wetting phenomena remain scarcely discussed in the literature for systems under pressure.

In the Young equation (1), the liquid/fluid interfacial tension (γ_{LF}) and the contact angle are directly measurable, unlike the solid/fluid interfacial tension (γ_{SF}) and the solid/liquid interfacial tension (γ_{SL}). On the one hand, contact angle is necessary for wettability characterization. On the other hand, it will enable the determination of further characteristics, such as the work of adhesion between given solid and liquid (W_{SL}) [17], or the critical surface tension of the solid (γ_C) [28–30], when coupled with liquid-fluid interfacial tension, or even the solid/liquid interfacial tension with several measurements on solid substrates of the same nature with various roughness [31]. Indeed, the work of adhesion can be calculated using the well-known Young-Dupré Equation by only knowing γ_{LF} and θ [17], while the critical surface tension of solid γ_C, which can be assimilated to γ_{SF}, can be determined with the Zisman's plot method [28,29] that requires the knowledge of both γ_{LF} and θ for a series of liquids. These characteristics are of further interest since they give information about solid/liquid interface and solid/fluid interface where γ_{SF} and γ_{SL} are not directly measurable. Afterwards, these properties are also required in various correlations used in chemical engineering. For instance, the correlation of Onda [32,33], used for the estimation of the wetted specific surface, includes the liquid-fluid interfacial tension as well as the critical surface tension of the solid γ_C.

In order to study the behavior of the wettability in saturated dense CO_2 media and complete a previous work on liquid/fluid interfacial tensions under the same conditions [34], contact angle measurements of ethanol, water and their mixtures were then realized on two stainless steel surfaces. The ethanol-water system has been previously described as a good model system, since several thermodynamic properties of both ethanol and water under pressure are well-documented in the literature [35–39]. Additionally, ethanol-water mixtures are of industrial interest, to produce highly concentrated ethanol solutions [40–43], or for alcoholic beverage treatment, using the $scCO_2$ fractionation process [44–46]. Considering the composition variation of ethanol-water mixture along the counter-current column in such processes, it is of interest to characterize the interfacial properties, like the contact angle, for several of these mixtures in contact with saturated dense CO_2. Besides, stainless steel was chosen as the solid substrate since it is the most common packing material used in supercritical fractionation because of its good resistance to corrosion, chemical inertness, and relatively inexpensive price. Although stainless steel is not ideal from a theoretical standpoint as it is a metal alloy with surface roughness, it holds significant practical importance in chemical engineering considering the widespread usage in various industries.

To the best of our knowledge, contact angle measurements on stainless steel surface in saturated dense CO_2 were carried out only with pure water or with pure ethanol [3–5] and no data were found in the literature regarding contact angles of ethanol-water mixtures. Therefore, an experimental campaign was carried out to measure the static contact angle by the sessile drop method of five solutions: ethanol, water, and three mixtures of different ethanol mass fractions, noted ω, of 0.25, 0.50 and 0.75, on stainless steel supports in contact with saturated dense CO_2 thanks to an original set-up enhancing mass transfer between the studied liquid and the continuous fluid phase. Experimental conditions for contact angle measurements were chosen to correspond to typical operating conditions applied in the fractionation of ethanol-water mixtures using $scCO_2$ [40–43], with pressures up to 15.1 MPa and temperatures of 313 K and 333 K. Besides, solid surface analyses were also realized to observe the morphology of the surfaces

as well as to measure their roughness. These characterizations enable the use of the Wenzel Equation to correct the observed contact angles by considering the roughness effect.

2. Materials and methods

2.1 Materials

Absolute ethanol (VWR Chemicals) with a purity higher than 99.8% and ultrapure water (Merck) with a resistivity of 18.2 MΩ·cm were used for contact angle measurements. Mixtures were prepared using the same reagents by weighing. This method was validated by density analysis with a densimeter Anton Paar DMA 4500. Three aqueous mixtures with ethanol mass fractions of 0.25, 0.5 and 0.75 were then studied. High grade CO_2 (Linde) was used during experiments with a purity greater than 99.9%.

Stainless steel surfaces (GoodFellow) used for contact angle measurements were made of 316 and 316L, following the American Iron and Steel Institute (AISI) nomenclature. They were shaped as a disc with a 1.5 mm diameter and a 0.5 mm thickness. The surface of a standard packing element InterPack® (VFF) in stainless steel was also analyzed to compare it with AISI 316 and 316L surfaces. The element could be in AISI 304, 304L, 316 or 316L according to VFF.

2.2 Contact angle measurement

One of the most common methods for static contact angle measurements under high-pressure is the sessile drop method [2,5,7,8]. The experimental setup allowing to realize these measurements under saturated dense CO_2 is presented in Figure 2, and was previously described for interfacial tension measurements [34,47]. For the contact angle measurements, a PEEK support (L) on which the stainless steel surface (K) is deposited (Figure 2.b), is introduced in the measurement cell (H).

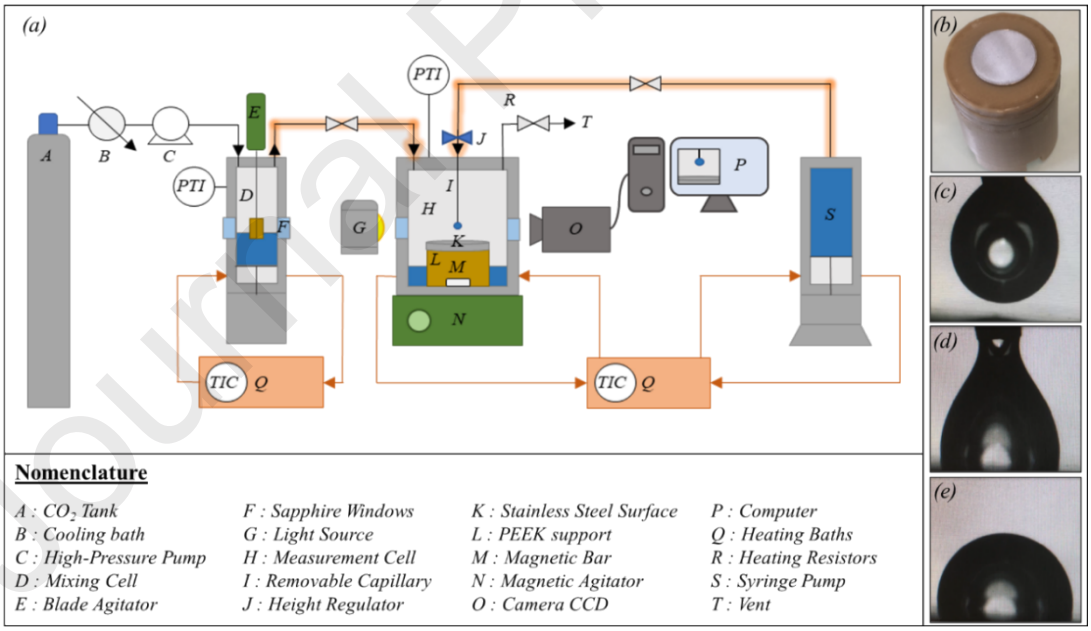

Figure 2 Experimental setup for contact angle measurements at elevated pressures and temperatures. (a) Schematic diagram; (b) PEEK support and stainless steel surface; (c) stabilized hanging drop; (d) contact between the drop and the studied surface; (e) drop deposited after the rise of the capillary

Contact angles were measured on AISI 316 and 316L for five liquids: ultrapure water, absolute ethanol, and three ethanol-water mixtures of ethanol mass fractions of 0.25, 0.50 and 0.75, in contact with CO_2 under different pressures from 0.1 to 15.1 MPa at two temperatures of 313 K and 333 K. Before starting contact angle experiments, stainless steel surfaces were cleaned with absolute ethanol, then dried with dry air flow to avoid surface contamination.

At the beginning, the mixing cell (D), of a maximal volume of 86 mL, and the measurement cell (H), of a volume of 48 mL, were filled with 50 mL and 5 mL of the studied solution, respectively. Large volumes of studied liquid were introduced in both cells to keep the equilibrium composition, obtained after mass transfer, close to the initial composition, especially in the case of ethanol-water mixtures. The syringe pump (S), of a 100 mL volume, was also filled with the studied solution. The set-up was then closed and flushed with CO_2 to remove the air and temperature and pressure were set. The CO_2 was "pre-saturated" with the studied solution by flowing through the mixing cell under agitation.

After 30 to 60 minutes of CO_2-rich phase saturation time, a drop was generated at the end of the removable capillary (I), with an internal diameter of 500 µm, using the syringe pump (S) with a low flowrate, around 1−2 $\mu L \cdot s^{-1}$. The drop volume was kept around 5 µL, and it was maintained for about ten minutes at the end of the capillary (Figure 2.c), to provide CO_2 transfer into the liquid phase [48]. If the system was not well saturated, some volutes were observed. Consequently, it is important to ensure sufficient saturation of the CO_2-rich phase to limit transfer from the drop to the bulk phase after its generation. The drop was then deposited on the stainless steel surface by descending the removable capillary (I), thanks to the height regulation (J), until contact between the drop and the surface (K) (Figure 2.d). The reverse operation with (I) was made to finally free the drop (Figure 2.e). Once the drop was deposited, several pictures were taken over time, for 15 to 30 min, to ensure the stability of the system that was then supposed to be at equilibrium or at least at a static state. Drop pictures were analyzed using FIJI software and the "contact angle measurement" plug-in developed by Brugnara [49]. Measurements, considered as apparent or observed contact angle, were realized at least in triplicate. These measures were then corrected with the Wenzel equation (Eq. (2)), and a mean value was finally calculated. The repeatability uncertainty was calculated for a 95% confidence level.

2.3 Surface characterization and correction of the observed contact angle

Observations of the morphology and the chemical uniformity of stainless steel surfaces were carried out, along with measurements of the roughness, developed surface (σ_d) and projected surface (σ_p) that define the roughness parameter ϕ, in equation (Eq. (3)). The roughness parameter is required in the application of the Wenzel equation (Eq. (2)), where the measured contact angle, or Wenzel apparent contact angle, is noted θ_w, and the corrected angle, referred as the Young contact angle, is noted θ [18]. The wetting is then assumed to be homogeneous.

$$cos\ \theta_W = \phi \cdot cos\ \theta \quad (2)$$

$$\phi = \frac{\sigma_d}{\sigma_p} \quad (3)$$

The morphology was observed using Scanning Electron Microscopy by Field Emission Gun (SEM-FEG) (Jeol JSM-7900F). Chemical uniformity of the metal alloy was also verified by X-ray spectroscopy analysis (BRUKER Esprit) using the same SEM-FEG. The roughness, expressed in Root Mean Square (RMS) in this work, the developed surface (σ_d), and the projected surface (σ_p) were determined in triplicate using Atomic Force Microscopy (AFM) for three different surface sizes (90×90, 30×30, 10×10 μm^2), with a resolution of 512×512 pixels, which is higher than the minimal resolution recommended in the literature [50]. However, AFM measurements for the InterPack® packing with the 90×90 μm^2 were not possible because of the curvature of the element. The average values were then considered. The AFM used in this work was an AFM Multimode Nanoscope III (Digital Instrument), in tapping mode with a Mikromasch HQ:NSC15/ Al BS, and the picture analysis was carried out with the software Gwyddion.

3. Results and discussion

3.1 Apparent contact angle, surface characteristics and roughness correction

Pictures of observed contact angles are presented in the supporting material (Appendix A) for both stainless steels in all explored conditions and are comprised between 20° and 130°, except for ethanol that shows total wetting. Similar behavior was previously observed in the literature on AISI 303 [5].

Stainless steel surface characterization results are presented in Figure 3 for the AISI 316, the AISI 316L and the InterPack® element. At low magnification, the surface appeared streaked for both 316 and 316L samples. At higher magnification, the steel grain was visible, and grain boundaries were finer for the AISI 316 than for the AISI 316L. Nonetheless, both samples appeared chemically uniform by X-ray spectroscopy, with a homogeneous repartition of the alloy compounds. From AFM characterization, the roughness was higher for AISI 316L than for AISI 316, respectively from 81 nm to 146 nm and from 33.5 nm to 131 nm according to the screened scale. The lower roughness at low scale corresponds to the roughness of the grain while the higher roughness at higher scale includes the streaking of the surface which generates these evolutions of the measured RMS. Although these roughness measurements were ten times bigger than the one obtained on stainless steel (AISI 304) with polishing treatment [2], the roughness remained quite low. Besides, morphology and AFM observations are in good agreement since AISI 316L stainless steel is rougher than AISI 316.

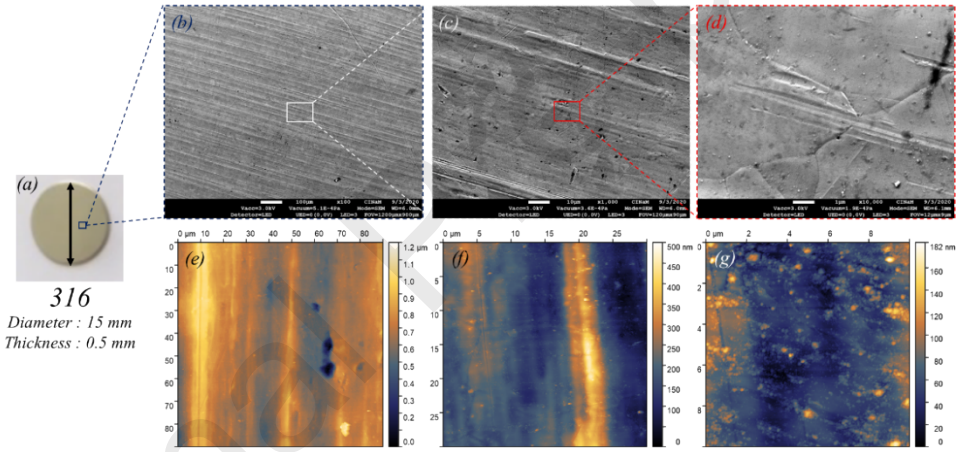

AISI 316			
Surface	**10x10 µm²**	**30x30 µm²**	**90x90 µm²**
RMS (nm)	*33.5 ± 1.4*	*98 ± 1.0*	*131.4 ± 1.7*
ϕ	*1.0374 ± 0.0066*	*1.0158 ± 0.0014*	*1.0051 ± 0.0020*

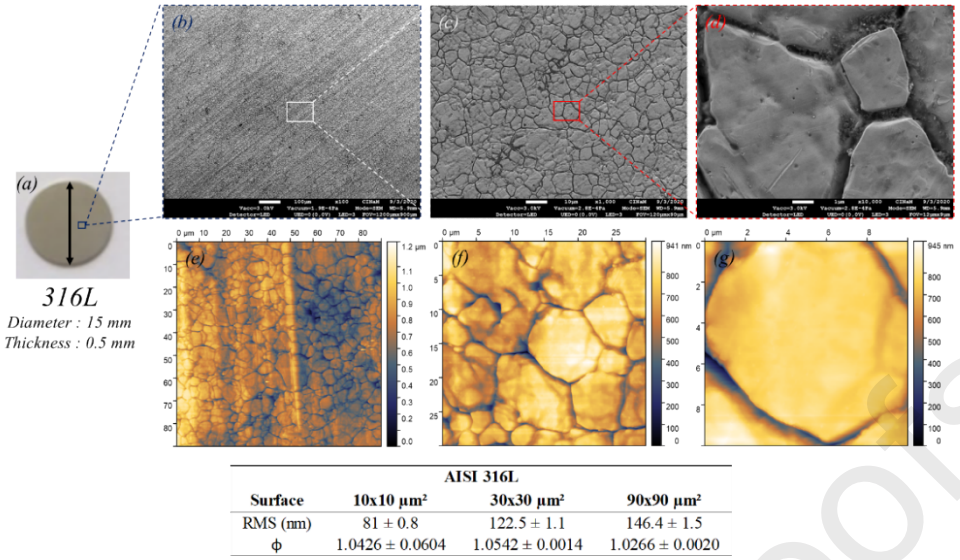

AISI 316L

Surface	10x10 µm²	30x30 µm²	90x90 µm²
RMS (nm)	81 ± 0.8	122.5 ± 1.1	146.4 ± 1.5
ϕ	1.0426 ± 0.0604	1.0542 ± 0.0014	1.0266 ± 0.0020

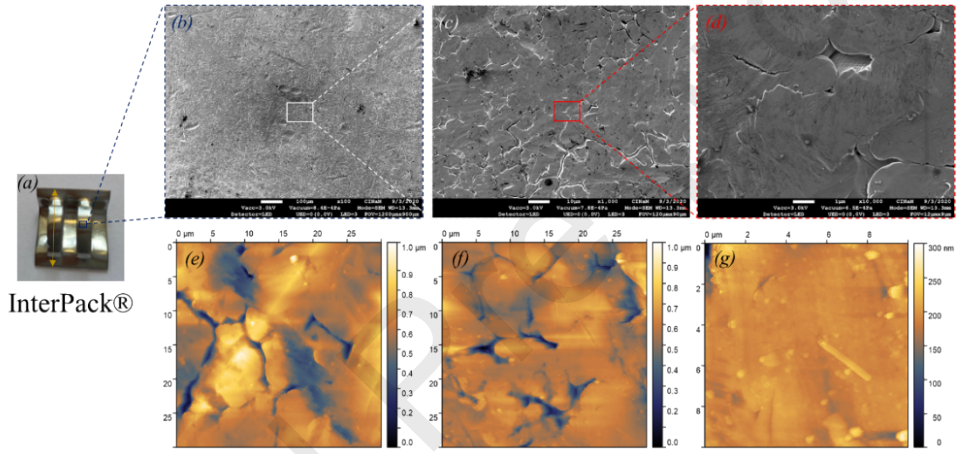

InterPack®

Surface	10x10 µm²	30x30 µm²
RMS (nm)	23.3 ± 1.1	102 ± 1.1
ϕ	1.0155 ± 0.0142	1.0257 ± 0.0061

Figure 3 Surface characterization of AISI 316, 316L and InterPack® element:
(a) sample picture; (b,c,d) SEM-FEG observations with magnification of ×100, ×1000 and ×10000, respectively;
(e,f,g) AFM observations; and table of AFM measurement results

The evolution of the roughness parameter ϕ for AISI 316 and 316L, from higher values at low scale to lower values at higher scale, was in accordance with previous literature [50]. Moreover, the significative uncertainty of the roughness parameter on the 10×10 µm² surface for AISI 316L (1.0426 ± 0.0604) was due to one of the measurements made on a grain of low roughness which was larger than the screened surface, lowering the average value and increasing the uncertainty. This behavior was not observed with the packing element with close values at both scales according to the uncertainties. To estimate the maximum of roughness effect, the biggest values of ϕ were used for the correction through the Wenzel equation for each surface with $\phi = 1.0374$ for AISI 316 and $\phi = 1.0541$ for AISI 316L, respectively. Even if the scales of AFM measurements were lower than the drop size, the retained values were expected to be representative of the three phase line contact characteristics.

The roughness effects described by Wenzel equation imply that the corrected contact angle (θ) is higher than the Wenzel apparent contact angle (θ_w) if $\theta_w < 90°$, while corrected contact angle (θ) is lower than the Wenzel apparent contact angle (θ_w) if $\theta_w > 90°$, and it remained ineffective if $\theta_w = 90°$ [17]. This behavior is illustrated in the supporting material (Appendix B) for the considered roughness factors of each stainless steel and apparent contact angles can be computed from these data.

3.2 Influence of pressure on contact angle in saturated dense CO_2

In this section, corrected average contact angles at each condition are presented in Figure 4. Each figure presents the contact angle at 313 K and 333 K on AISI 316 and 316L for water (Figure 4.a), and the three studied ethanol-water mixtures (Figure 4.b-d). All data are presented in supporting material (Appendix C).

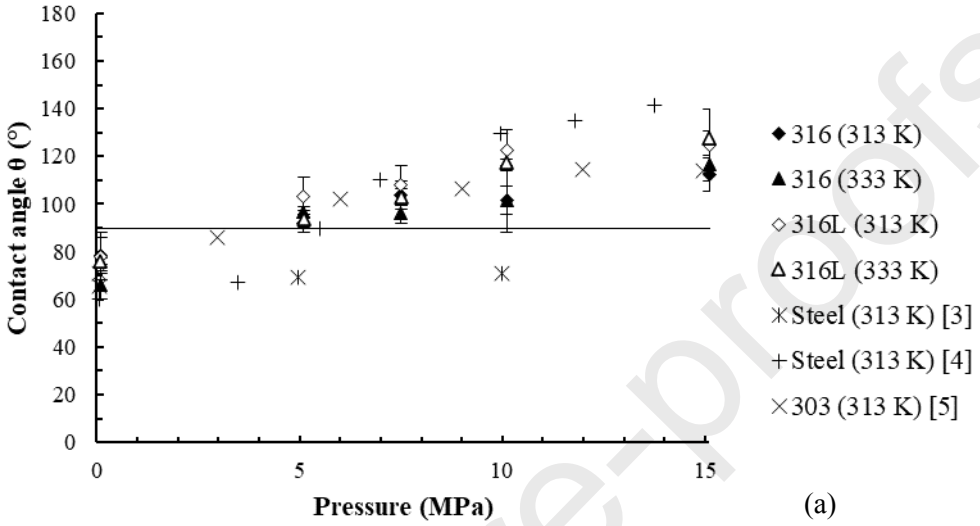

(a)

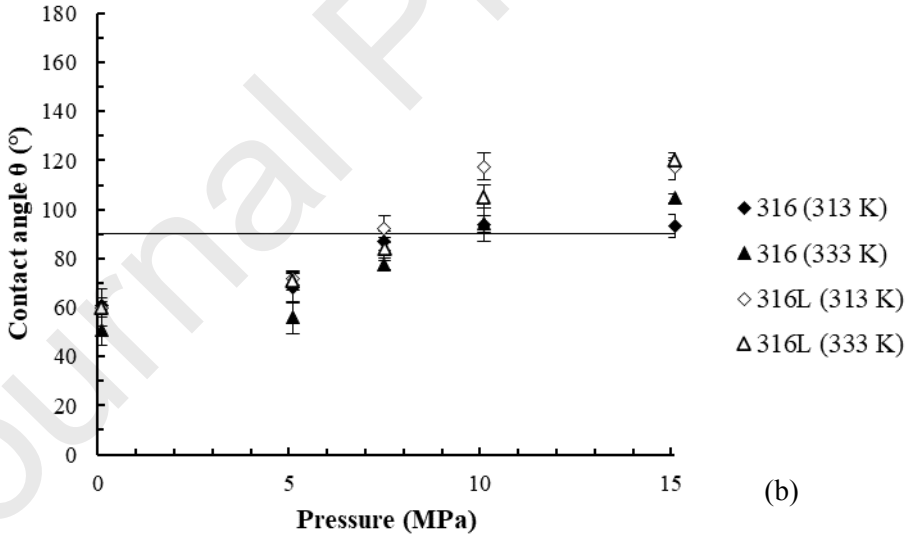

(b)

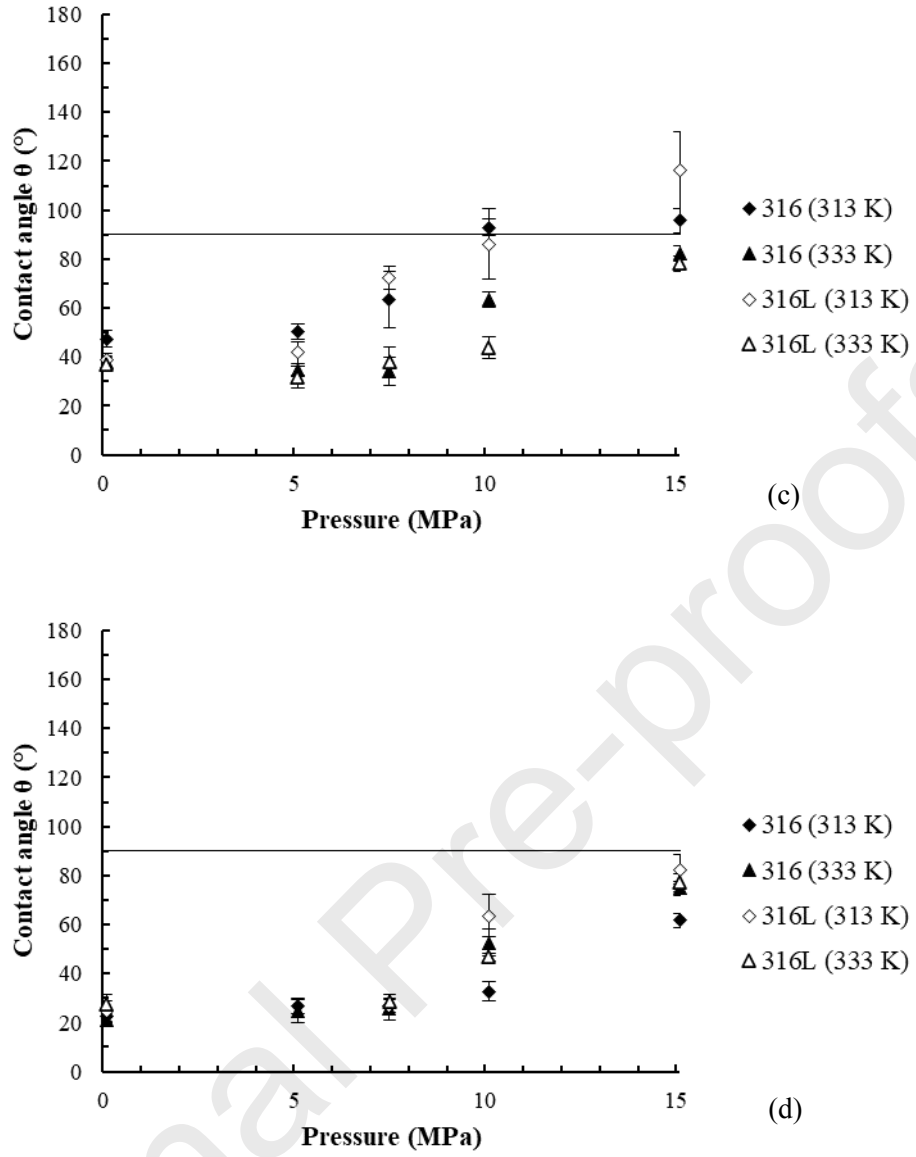

Figure 4 Contact angle as a function of pressure at 313 K and 333 K on AISI 316 or AISI 316L for (a) water (on AISI 303 or on unknown type of steel at 313 K [3–5]); and of ethanol-water mixtures: (b) ω = 0.25; (c) ω = 0.50; (d) ω = 0.75

Ethanol contact angle on stainless steel AISI 316 and 316L in dense saturated CO_2

Ethanol drop formation with the capillary was not possible for pressures higher than around 8 MPa at 313 K and higher than around 10 MPa at 333 K, because the system ethanol/CO_2 is miscible beyond these conditions and becomes monophasic [34]. Hence, operating conditions were restricted for ethanol. Ethanol totally wetted the stainless steel surfaces (AISI 316 and 316L), forming a liquid film on the solid surface instead of a drop, for all explored conditions (Appendix A, Figure 6). A similar behavior was reported by Sutjiadi-Sia *et al.* [5] concerning ethanol wettability on AISI 303 in dense CO_2 at 313 K.

Water contact angle on stainless steel AISI 316 and 316L in dense saturated CO_2

Contact angle of water on AISI 316 and AISI 316L as a function of pressure is presented in Figure 4.a with available literature data [3–5]. The contact angle of water was increased by the rise of pressure reaching maximal values of 128° and 125° on AISI 316L at 333 K and 313 K, respectively. Measurements are in good agreement with the work of Sutjiadi-Sia *et al.* [5], despite the difference of stainless steel (AISI 303). In contrast, contact angles of water on steels presented in [3,4] presented some

discrepancies. As discussed by Sutjiadi-Sia [51], discrepancies observed in the work of Jaeger [4] could be the result of different measurement methods, while much lower values observed by Wesch *et al.* [3] could be generated by different wetting characteristics of the studied steel since the water wets it with contact angles lower than 90° for pressures up to 10 MPa. Nonetheless, this study, along with the studies of Sutjiadi-Sia *et al.* [5] and Jaeger [4] remain in the same order of magnitude, despite the stainless steel difference, indicating that these values could be representative of the general behavior of the water contact angle in dense saturated CO_2 on standard stainless steel (without specific treatment).

Influence of pressure was the same at both studied temperatures according to the stainless steel support. When the pressure increased, the contact angle of water also increased. At 0.1 MPa, water wetted the material with contact angles less than 90° while non-wetting behavior was observed for higher pressures (≥ 5.1 MPa) with angles up to around 112° to 128° at the highest pressure. This behavior was also reported in the work of Sutjiadi-Sia *et al.* [5] which is followed by the stabilization of the water contact angle for higher pressure, up to 27 MPa at 313 K.

This behavior according to the pressure can be understood in terms of interfacial tensions of the system with the Young equation rearranged and written in the form of Equation (4), completed with assumptions made from other works.

$$cos\ \theta_Y(P) = \frac{\gamma_{SF}(P) - \gamma_{SL}(P)}{\gamma_{LF}(P)} = \frac{\gamma_{SF}(P)}{\gamma_{LF}(P)} - \frac{\gamma_{SL}(P)}{\gamma_{LF}(P)} \quad (4)$$

Data on γ_{SF} for stainless steel (AISI 303) in contact with dense CO_2 can be found in the work of Sutjiadi-Sia *et al* [52] at 313 K and up to 27 MPa. These data have been determined in a system involving sessile drops of water and ethanol on stainless steel in dense CO_2. Moreover, data of water/CO_2 interfacial tension are also available in the literature at 313 K [34], allowing the calculation of the γ_{SF}/γ_{LF} ratio in the equation (4). At 313 K, this ratio first decreases then becomes almost constant between 10 MPa and 15 MPa (Appendix D).

Estimation of γ_{SL} is scarce in the literature and no data were found for CO_2/water/stainless steel system. Nonetheless, the interfacial tension γ_{SL} was estimated to be constant or increasing with a pressure rise by Dickson *et al.* [26] for the CO_2/water/glass system at 296 K, corresponding to subcritical conditions for CO_2. Hence, the ratio γ_{SL}/γ_{LF} can be assumed to increase with a pressure rise at 313 K, if γ_{SL} is constant or increasing since γ_{LF} is known to be decreasing with pressure [34]. Following these assumptions, the ratio difference (γ_{SF}/γ_{LF} - γ_{SL}/γ_{LF}) leads to a decrease of $cos\theta_Y$ which corresponds to an increase in θ_Y with the pressure rise. Moreover, if both ratios became constant for higher pressure, then the contact angle would also be constant, as observed in the work of Sutjiadi-Sia *et al.* [5].

Ethanol-water mixtures contact angle on stainless steel AISI 316 and 316L in dense saturated CO_2

Contact angles of ethanol-water mixtures are presented in Figure 4.b,Figure 4.c andFigure 4.d, for mixtures with ethanol mass fractions ω of 0.25, 0.50 and 0.75, respectively. No previous data were found in the literature to compare with the results of this work.

Concerning the pressure influence, contact angle of all mixtures increased when pressure increased. This behavior could be generated by the evolution of the interfacial tension balance as presented for water. However, the contact angle of the mixture with low ethanol content (ω = 0.25) showed at first an increase, up to around 10.1 MPa, and then seemed to stabilize. This behavior is similar to the behavior obtained with the water.

In contrast, the contact angle of mixtures of medium and high ethanol contents (ω = 0.50 and ω = 0.75) as function of pressure was almost constant or showed a small rise at first, up to around 5.1−7.5 MPa, which was followed by a significant increase at higher pressures, and no stabilization was observe in

this operating condition range. Several assumptions can be made to discuss these observations. First, it is important to note that the composition of both the liquid and the fluid phases are determined by the Vapor-Liquid equilibrium (VLE). Hence, both phases became a mixture of the three compounds CO_2, ethanol, and water, after the mass transfer occurred. Consequently, the composition of the sessile drop can deviate from the composition of the initial mixture. On the one hand, CO_2 will transfer inside of the drop [5]. On the other hand, ethanol will preferentially transfer towards CO_2-rich phase since it has more affinity for $scCO_2$ than water, leading to the rise of the water content in the drop and higher contact angles. This latter phenomenon will be more significative at higher pressure when the density and the solvent power of the CO_2 are increased. As perspective, experimental set-up allowing the knowledge of the global composition of the system to determine the VLE data in given conditions would allow the determination of the effective content of each compound in the drop as well as in the fluid phase. Second, a potential heterogeneity of the liquid/solid interface due to trapped bubbles could also play a role in the apparent contact angle as initially reported in the work of Cassie and Baxter [21]. Indeed, the presence of such bubbles could indicate a switch from homogeneous wetting to heterogenous wetting by increasing the pressure. This effect is discussed in further details in section 3.5.

3.3 Influence of temperature and stainless steel surface

The temperature seemed to have a low influence for both AISI 316 and 316L in the tested temperature range (313 K and 333 K). This is in accordance with the work of Song *et al.* [2] which deals with water contact angle on stainless steel in N_2 for high pressure and high temperature. Indeed, three temperature dependent regimes were described: low temperature (< 393 K); intermediate temperature (393 K < T < 483 K); and high temperature (T > 483 K) [2]. The low temperature regime, that corresponds to the conditions applied here, showed a weak decrease in the contact angle generated by a temperature increase, which is the mostly observed in this work (Figure 4). Nonetheless, the temperature dependence in the case of the mixture containing 0.5 mass fraction of ethanol is more pronounced. Indeed, the increase of temperature from 313 K to 333 K led clearly to a lower contact angle for both stainless steels. This behavior could be due to the higher CO_2 density at 313 K than at 333 K, increasing the solvent power of the CO_2 and modifying the drop composition towards higher water content at 313 K than at 333 K, as discussed in the section 3.2. Nonetheless, no such temperature dependence was observed for the mixture with an ethanol mass fraction of 0.75. Besides, the discussion in terms of interfacial tension balance with the Young equation (Eq. (1)) is not possible since data were found only for γ_{LF} at various temperatures and not for γ_{SL} and γ_{SF}.

Small differences remain observable between contact angles on AISI 316 and AISI 316L despite the correction of the contact angle through the Wenzel equation. If the contact angle magnitude were similar for both stainless steels, slightly higher contact angles were generally observed on 316L (Figure 4). The difference could be explained by the difference of the global chemical composition of the two stainless steels 316 and 316L; nevertheless, this difference only consisted of a small amount of carbon. Besides, the difference could be attributed to the chemical heterogeneity of the solid/liquid interface generated by trapped bubbles that is discussed in section 3.5.

Because of measurement uncertainties, the temperature and the stainless steel surface influences required further measurements to be confirmed. Measurements on ideal surface under larger temperature range remain of interest to discuss the temperature influence on contact angles in saturated dense CO_2.

3.4 Influence of ethanol mass fraction

Contact angle as a function of ethanol mass fraction for pressures from 0.1 MPa to 15.1 MPa are presented at 313 K in Figure 5.a andFigure 5.b and at 333 K in Figure 5.c andFigure 5.d for 316 and 316L surfaces, respectively. Since ethanol totally wetted on both stainless steels, the contact angle values were supposed to be zero for pressures up to 7.5 MPa at 313 K and up to 10.1 MPa at 333 K. Beyond these conditions, the ethanol/CO_2 system is miscible in all proportions and becomes monophasic[34].

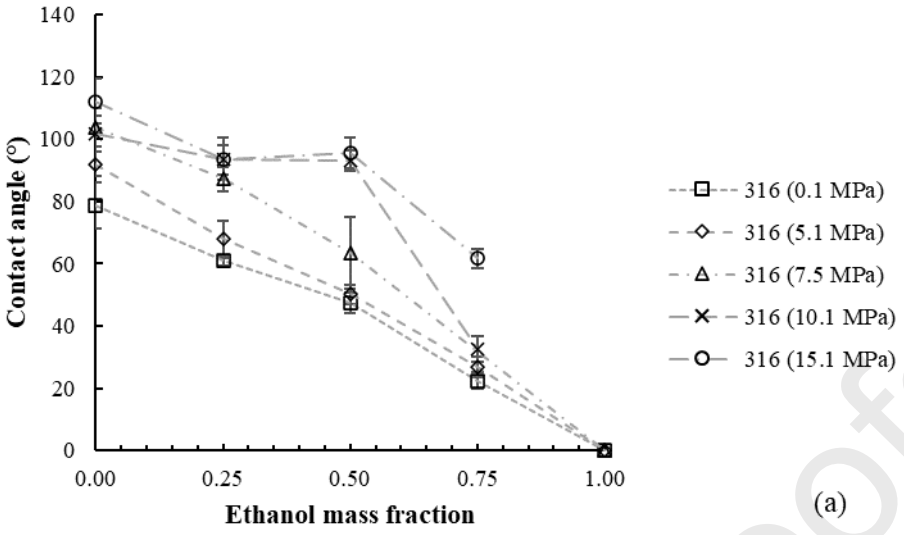

(a)

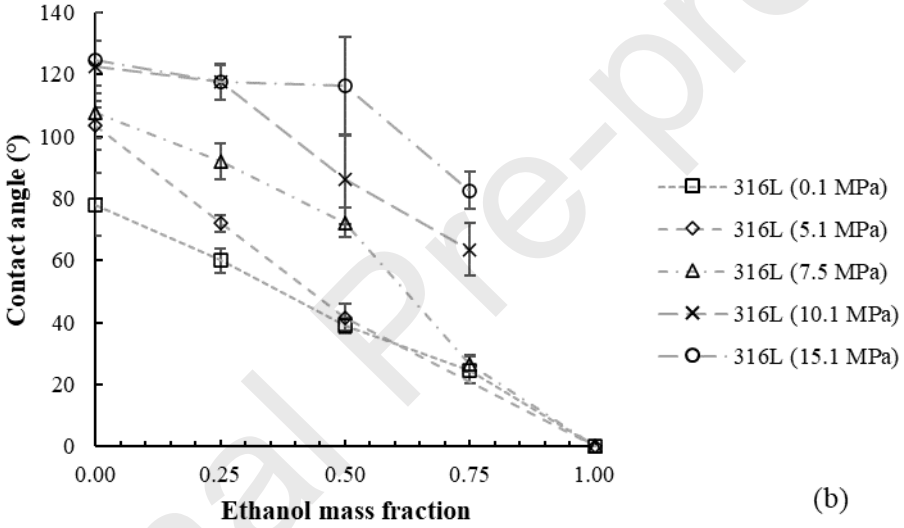

(b)

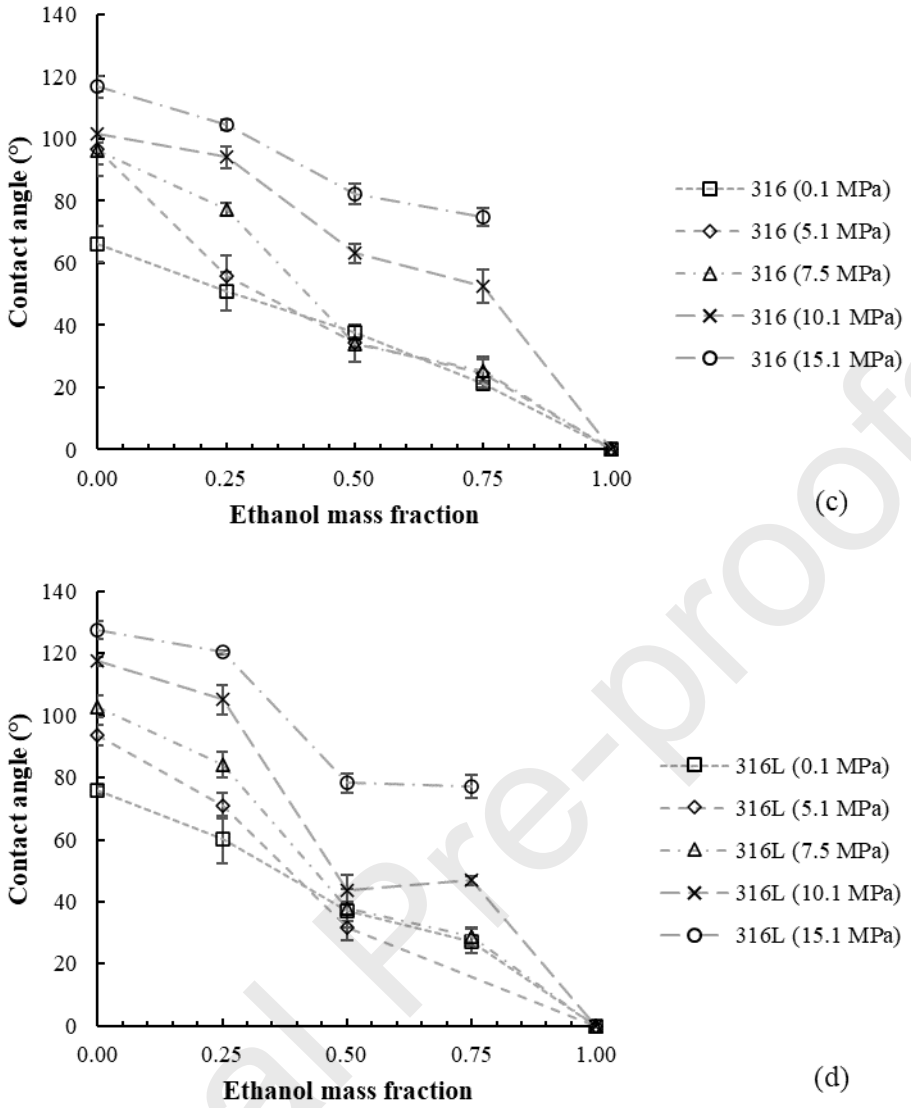

Figure 5 Contact angle as a function of ethanol mass fraction at various pressures: (a) 316 at 313 K, (b) 316L at 313 K, (c) 316 at 333 K and (d) 316L at 333 K, dotted lines are plotted to guide the eye

As a general behavior, the contact angle diminished as the ethanol mass fraction increased. Similar tendencies of ethanol-water mixture contact angle on different types of glass as a function of ethanol mass fraction have been also observed in air [53]. For pressures under 7.5 MPa, corresponding to the gaseous state of the CO_2, the decrease was quite linear. However, the evolution of the contact angle through the ethanol mass fraction seemed not monotonic at higher pressures, where the CO_2 is beyond its critical point. The observed behavior of the contact angle at higher pressures can then be the result of transfer phenomena with lower ethanol content in the mixture drops and higher contact angles, together with a potential influence of surface heterogeneity, as discussed in the following section 3.5.

Besides, the liquid/fluid interfacial tension γ_{LF} of ethanol-water mixtures is known to decrease exponentially with a rise of ethanol content [34], which results in a diminishing denominator in the Young equation (4). Nonetheless, no information is available concerning the evolution of γ_{SL} with the variation of the ethanol content of the system. Furthermore, the composition of the CO_2-rich phase depends on the nature and the amount of liquid in contact with, which could also modify the solid/fluid interfacial tension γ_{SF} according to the studied liquid. However, the contact angle behavior suggests that the γ_{LF} decreases more significantly than the term (γ_{SF} - γ_{SL}) with a rise in ethanol content since smaller contact angles are obtained.

3.5 Discussion on influence of surface heterogeneity and adsorbed film

Trapped bubbles were observed at the liquid/solid interface during several measurements at pressures of 10.1 MPa and 15.1 MPa, mainly for ethanol mass fractions of 0.75 and 0.50 (Appendix E). The formation of bubbles could be generated by trapped fluid in the solid asperities. Nonetheless, another phenomenon could be relevant in the formation of bubbles at the solid/liquid interface such as the oversaturation of dissolved fluid in the liquid phase at the solid/liquid interface as indicated by Tortora *et al.* [54] in the case of nanobubble formation. Since the solubility of CO_2 in water [5] and ethanol [55] increases with pressure, the latter phenomenon could be enhanced at higher pressures. Then, the formation of macroscopic bubbles could be formed by coalescence.

The presence of trapped bubbles could also indicate a potential chemical heterogeneity of the solid/liquid interface. The wetting regime could then evolve depending on the operating conditions, switching from homogenous wetting at low pressure to heterogeneous wetting at higher pressure. The determination of the wetting regime (homogeneous or heterogenous) is generally solved by a minimization of the Gibbs energy of the system [56], and the transition between homogenous and heterogenous wetting has been discussed in terms of energy barrier in the literature [57]. The Gibbs energy of the system, noted G, is generally given by the equation (Eq. (5)), where γ and A are the interfacial tensions and interfacial areas, respectively, at the interfaces liquid/fluid (LF), solid/liquid (SL) and solid/fluid (SF) [56].

$$\boldsymbol{G = \gamma_{LF} \cdot A_{LF} + \gamma_{SL} \cdot A_{SL} + \gamma_{SF} \cdot A_{SF}} \quad (5)$$

The modification of interfacial tensions through pressure will then influence both the Gibbs energy of the system and the energy barrier required for the wetting regime transition. To discuss the potential influence of the surface heterogeneity, the Cassie-Baxter equation (Eq. (6)) is considered.

$$\boldsymbol{\cos\theta_{C-B} = \sigma \cdot \cos\theta + \sigma_2 \cdot \cos\theta_{CO_2} \leftrightarrow \cos\theta_{C-B} = \sigma \cdot (\cos\theta + 1) - 1} \quad (6)$$

The contact angle θ_{C-B} corresponds to the observed contact angle and θ to the corrected contact angle. The heterogeneity is considered through the σ parameter, that corresponds to the fraction of the solid surface wetted by the liquid; and σ_2, the fraction of the surface formed by the trapped gas, or saturated dense CO_2. The total surface is generally normalized to obtain $\sigma + \sigma_2 = 1$; *and* $\theta_{CO_2} = 180°$. The parameter σ is not known in this work, and heterogeneity can only be prospected using equation (6). Values of corrected contact angle from equation (6) using different arbitrary values of σ from 0.9 to 1 are then presented in the supporting material (Appendix E) to illustrate the influence of solid/liquid interface heterogeneity. This model describes a significant increase in the apparent contact angle with a diminution of σ, especially for smaller contact angles, and even for a low fraction of non-wetted solid surface.

Because the phenomenon of trapped bubbles was observable mainly with mixtures of 0.50 and 0.75 ethanol mass fractions, two assumptions can be made. First, the rise of the contact angle of mixtures with ethanol mass fractions of 0.50 and 0.75 observed at high pressure could be interpreted, in part, as an effect of enhanced surface heterogeneity in these conditions. Second, the bubble trapping, and thus potential switch from homogeneous wetting to heterogeneous wetting, could be favored by the low liquid/fluid interfacial tension γ_{LF} of these mixtures [34].

The roughness is also known to influence the wetting regime, with for instance preferential heterogeneous wetting above a certain value of the roughness factor for sinusoidal surface [56]. The height of asperities has also been pointed out as influencing their capability to entrap air pocket [58], indicating that a rougher surface can promote the bubble trapping. Moreover, asperities favor the nucleation of bubbles [8]. Hence, the surface heterogeneity of AISI 316L could be greater than the

surface heterogeneity of the AISI 316, since the 316L is rougher than the 316. This assumption can explain, in part, the difference between contact angles on both surfaces with generally higher values on AISI 316L, especially at pressures of 10.1 MPa and 15.1 MPa. Further works on various well-defined surfaces with controlled roughness or patterning should clarify the influence of roughness and heterogeneity under saturated dense CO_2 atmosphere, which is scarcely discussed in the literature, and even highlight the possibility of a wetting regime transition generated by the rise of pressure [56,57,59,60].

Besides, the existence of an adsorption layer on the solid surface has been underlined as influencing its wettability [23–25,61]. The solid/fluid interfacial tension for the stainless steel/CO_2 system is greatly reduced with a pressure rise, as concluded by Sutjiadi-Sia *et al.*[52]. This diminution of γ_{SF} could then be interpreted as the result of the formation of the adsorption layer on the stainless steel. However, since mass transfer occurs between the CO_2-rich phase and the liquid phase [5], the exact nature, molecular composition and thickness, of such adsorbed film in saturated dense CO_2 remains unknown although assumed of great influence by Santos *et al.*[8].

4. Conclusions and perspectives

This work brings experimental measurements of contact angle on two types of stainless steel surfaces, in AISI 316 and 316L, of absolute ethanol, ultrapure water and newly for three of their mixtures (with ethanol mass fraction of $\omega = 0.25$; $\omega = 0.50$ and $\omega = 0.75$) in saturated dense CO_2 atmosphere from 0.1 MPa to 15.1 MPa at 313 K and 333 K. Experiments were carried out in an original set-up allowing enhanced mass transfer between the studied liquid and the continuous fluid phase. Moreover, surface characteristics, morphology, homogeneity of the metal alloy, roughness and roughness parameter were also determined thanks to SEM observations and AFM measurements. Such characterization enables the use of the Wenzel equation (Eq. (2)) describing the roughness effect on apparent contact angle that are often neglected for measurements under high-pressure. Experimental conditions were restricted for ethanol to pressure up to 8 MPa at 313 K and 10.1 MPa at 333 K because of the miscibility in all proportions of the ethanol/CO_2 system which becomes monophasic [34]. Ethanol showed total wetting on both stainless steels at each experimental condition that is in accordance with previous literature [5]. Contact angles of water increased with pressure rise on both stainless steels at both temperatures. This behavior was previously described in the literature for this pressure range but seems to stabilize at higher pressure, up to 27 MPa [5]. The rise of the water contact angle through pressure, as well as its stabilization at higher pressure, appeared in agreement with the Young equation considering the hypothesized evolution of the balance of the interfacial tensions. Evolution of the ethanol-water mixture contact angle through pressure is different according to the mixture. Indeed, the behavior of the low ethanol content mixture ($\omega = 0.25$) followed the same tendency than water. In contrast, contact angles of mixture with medium and high ethanol content ($\omega = 0.50$ and $\omega = 0.75$, respectively) showed at first a low increase for pressure below around 5.1 MPa to 7.5 MPa while significant increases were observed at higher pressure and no stabilization seemed to appear (Figure 4). The rise of temperature from 313 K to 333 K seemed to decrease the contact angle despite the short range of temperature coupled with measurement uncertainties. Nonetheless, this behavior appeared clearly for the mixture with medium ethanol content ($\omega = 0.50$) and is in accordance with observed tendency for water contact angle on stainless-steel under pressurized N_2 [2]. Further measurements on ideal surface screening larger temperature range should be of interest to precisely discuss the temperature effect under saturated dense CO_2. Measurements on both stainless steels showed generally higher contact angle on AISI 316L than on AISI 316, especially under high pressure conditions. The increase of ethanol content in the liquid led to a decrease in the contact angle that appears quite linear for pressure up to 7.5 MPa, while non-monotonic behavior was observed at higher pressures, on both stainless steels and at both temperatures.

Several phenomena have been discussed according to the behavior of the contact angle through pressure, temperature, stainless steel surface and ethanol content of the studied liquid. It has been highlighted that transfer phenomena may play a role particularly at higher pressure by decreasing the ethanol content of the studied mixture leading to higher contact angles, since the density and the solvent power of CO_2, preferentially towards ethanol, are increased. The quantification of the mass transfer effect should be accessible by VLE calculation. Moreover, although the wetting was assumed homogeneous with the consideration of the roughness effect through the Wenzel equation (Eq. (2)), the observation of trapped bubbles at the solid/liquid interface suggested a potential heterogeneous wetting. The formation of bubbles could be generated from trapped fluid in the surface asperities and by an oversaturation of dissolved CO_2 in the liquid phase at the solid/liquid interface. Hence, the idea of a transition from homogeneous wetting to heterogeneous wetting induced by the rise of pressure, involving the diminution of the solid/fluid and the liquid/fluid interfacial tensions, is discussed according to the minimization of the Gibbs energy of the system. The potential influence of the surface heterogeneity is then discussed according to the Cassie-Baxter equation (Eq. (6)) that describes higher apparent contact angles in the case of heterogenous wetting. The influence of surface heterogeneity could then be involved in the significant increase of the contact angle of medium and high ethanol content mixtures observed through pressure. As well, rougher surface could involve higher surface heterogeneity and then higher apparent contact angles as observed on the AISI 316L that is rougher than the AISI 316. Also, trapped bubbles were mainly observable with medium and high ethanol content mixtures which could suggest higher surface heterogeneity enhanced by lower liquid/fluid interfacial tension generated by the increased ethanol content. Nonetheless, such wetting transition requires further investigation to be confirmed. Furthermore, the nature of the adsorption layer on stainless steel is a topic of interest since it has been less studied in literature and probably has an influence on the wettability. Besides, a first consequence of such adsorption layer under high pressure seems to be the decrease in the solid/fluid interfacial tension, as estimated in the work of Sutjiadi-Sia *et al.* [52].

As perspectives, the contact angle measurements of such solutions are also of interest for the calculation of the work of adhesion, with the well-known Young-Dupré equation, or even for the determination of the critical surface tension of the solid, thanks to the Zisman's plot method. Estimation of such parameters is also of interest in chemical engineering since they are directly required in usual correlations used for the estimation of mass transfer coefficients in the modeling and the simulation of several processes [32,33], such as $scCO_2$ fractionation of liquid mixture that is considered as a promising green process. Moreover, interfacial properties are pointed out to influence flooding phenomena in counter-current columns involving a dense gas or a supercritical fluid phase [9–13] and where a lack of data has been identified to discuss it. Further with respect to fractionation process, it is often emphasized that the range of operation pressure is narrow to keep enough density difference between the two phases to allow counter-current flows. This work shows also that lower pressures are recommended for higher packing wettability and higher contact area between the two phases for an enhanced mass transfer.

Acknowledgment

We warmly thank Laurent Lapena, from the Interdisciplinary Center of Nanoscience of Marseille (CINaM), for his grateful help.

References

[1] J.H. Clark, S.J. Tavener, Alternative Solvents: Shades of Green, Org. Process Res. Dev. 11 (2007) 149–155. https://doi.org/10.1021/op060160g.

[2] J.-W. Song, D.-L. Zeng, L.-W. Fan, Temperature dependence of contact angles of water on a stainless steel surface at elevated temperatures and pressures: In situ characterization and thermodynamic analysis, Journal of Colloid and Interface Science. 561 (2020) 870–880. https://doi.org/10.1016/j.jcis.2019.11.070.

[3] A. Wesch, N. Dahmen, K. Ebert, J. Schön, Grenzflächenspannungen, Tropfengrößen und Kontaktwinkel im Zweiphasensystem H2O/CO2 bei Temperaturen von 298 bis 333 K und Drücken bis 30 MPa, Chemie Ingenieur Technik. 69 (1997) 942–946. https://doi.org/10.1002/cite.330690709.

[4] P.T. Jaeger, Grenzflächen und Stofftransport in verfahrenstechnischen Prozessen am Beispiel der Hochdruck-Gegenstromfraktionierung mit überkritischem Kohlendioxid, PhD thesis, Technische Universität Hamburg-Harburg, 1998.

[5] Y. Sutjiadi-Sia, P. Jaeger, R. Eggers, Interfacial phenomena of aqueous systems in dense carbon dioxide, The Journal of Supercritical Fluids. 46 (2008) 272–279. https://doi.org/10.1016/j.supflu.2008.06.001.

[6] A. Bejarano, P.C. Simões, J.M. del Valle, Fractionation technologies for liquid mixtures using dense carbon dioxide, The Journal of Supercritical Fluids. 107 (2016) 321–348. https://doi.org/10.1016/j.supflu.2015.09.021.

[7] E. Santos, P.R. Waghmare, F. Temelli, Interfacial tension and equilibrium contact angle of corn oil on polished stainless steel in supercritical CO2 and N2, The Journal of Supercritical Fluids. 156 (2020) 104665. https://doi.org/10.1016/j.supflu.2019.104665.

[8] E. Santos, P.R. Waghmare, F. Temelli, Interfacial tension and equilibrium contact angle of lipids on polished glass in supercritical CO2, The Journal of Supercritical Fluids. 181 (2022) 105486. https://doi.org/10.1016/j.supflu.2021.105486.

[9] R. Stockfleth, G. Brunner, Hydrodynamics of a Packed Countercurrent Column for the Gas Extraction, Ind. Eng. Chem. Res. 38 (1999) 4000–4006. https://doi.org/10.1021/ie990251k.

[10] R. Stockfleth, G. Brunner, Holdup, Pressure Drop, and Flooding in Packed Countercurrent Columns for the Gas Extraction, Ind. Eng. Chem. Res. 40 (2001) 347–356. https://doi.org/10.1021/ie000466q.

[11] R. Stockfleth, G. Brunner, Film Thickness, Flow Regimes, and Flooding in Countercurrent Annular Flow of a Falling Film at High Pressures, Ind. Eng. Chem. Res. 40 (2001) 6014–6020. https://doi.org/10.1021/ie0100885.

[12] A. Pieck, C. Crampon, A. Fabien, E. Badens, A new correlation for predicting flooding point in supercritical fractionation packed columns, The Journal of Supercritical Fluids. 179 (2021) 105404. https://doi.org/10.1016/j.supflu.2021.105404.

[13] H.H. Franken, J.H. Knoetze, C.E. Schwarz, Influence of fluid properties on the hydrodynamics and operability of a countercurrent supercritical packed column, Chemical Engineering Research and Design. 159 (2020) 592–604. https://doi.org/10.1016/j.cherd.2020.05.009.

[14] J.-W. Song, L.-W. Fan, Understanding the effects of pressure on the contact angle of water on a silicon surface in nitrogen gas environment: Contrasts between low- and high-temperature regimes, Journal of Colloid and Interface Science. 607 (2022) 1571–1579. https://doi.org/10.1016/j.jcis.2021.09.021.

[15] T. Young, III. An essay on the cohesion of fluids, Philosophical Transactions of the Royal Society of London. 95 (1805) 65–87. https://doi.org/10.1098/rstl.1805.0005.

[16] R. Tadmor, Line Energy and the Relation between Advancing, Receding, and Young Contact Angles, Langmuir. 20 (2004) 7659–7664. https://doi.org/10.1021/la049410h.

[17] J.N. Israelachvili, 17 - Adhesion and Wetting Phenomena, in: J.N. Israelachvili (Ed.), Intermolecular and Surface Forces (Third Edition), Third Edition, Academic Press, San Diego, 2011: pp. 415–467. https://doi.org/10.1016/B978-0-12-375182-9.10017-X.

[18] P.-G. de Gennes, F. Brochard-Wyart, D. Quere, Capillarity and Wetting Phenomena: Drops, Bubbles, Pearls, Waves, Springer-Verlag, New York, 2004. https://doi.org/10.1007/978-0-387-21656-0 SMASH.

[19] G. Whyman, E. Bormashenko, T. Stein, The rigorous derivation of Young, Cassie Baxter and Wenzel equations and the analysis of the contact angle hysteresis phenomenon, Chemical Physics Letters. 450 (2008) 355–359. https://doi.org/10.1016/j.cplett.2007.11.033.

[20] S. Sarkar, T. Roy, A. Roy, S. Moitra, R. Ganguly, C.M. Megaridis, Revisiting the supplementary relationship of dynamic contact angles measured by sessile-droplet and captive-bubble methods: Role of surface roughness, Journal of Colloid and Interface Science. 581 (2021) 690–697. https://doi.org/10.1016/j.jcis.2020.07.098.

[21] A.B.D. Cassie, S. Baxter, Wettability of porous surfaces, Trans. Faraday Soc. 40 (1944) 546–551. https://doi.org/10.1039/TF9444000546.

[22] L. Gao, T.J. McCarthy, How Wenzel and Cassie Were Wrong, Langmuir. 23 (2007) 3762–3765. https://doi.org/10.1021/la062634a.

[23] D.H. Bangham, R.I. Razouk, Adsorption and the wettability of solid surfaces, Trans. Faraday Soc. 33 (1937) 1459–1463. https://doi.org/10.1039/TF9373301459.

[24] N.K. Adam, H.K. Livingston, Contact Angles and Work of Adhesion, Nature. 182 (1958) 128–128. https://doi.org/10.1038/182128a0.

[25] W.A. Zisman, INFLUENCE OF CONSTITUTION ON ADHESION, Ind. Eng. Chem. 55 (1963) 18–38. https://doi.org/10.1021/ie50646a003.

[26] J.L. Dickson, G. Gupta, T.S. Horozov, B.P. Binks, K.P. Johnston, Wetting Phenomena at the CO2/Water/Glass Interface, Langmuir. 22 (2006) 2161–2170. https://doi.org/10.1021/la0527238.

[27] L. Makkonen, A thermodynamic model of contact angle hysteresis, The Journal of Chemical Physics. 147 (2017) 064703. https://doi.org/10.1063/1.4996912.

[28] W.A. Zisman, Relation of the Equilibrium Contact Angle to Liquid and Solid Constitution, in: Contact Angle, Wettability, and Adhesion, AMERICAN CHEMICAL SOCIETY, 1964: pp. 1–51. https://doi.org/10.1021/ba-1964-0043.ch001.

[29] J.R. Dann, Forces involved in the adhesive process: I. Critical surface tensions of polymeric solids as determined with polar liquids, Journal of Colloid and Interface Science. 32 (1970) 302–320. https://doi.org/10.1016/0021-9797(70)90054-8.

[30] Y. Yonemoto, T. Kunugi, Estimating critical surface tension from droplet spreading area, Physics Letters A. 384 (2020) 126218. https://doi.org/10.1016/j.physleta.2019.126218.

[31] S. Sarkar, M. Jafari Gukeh, T. Roy, H. Gaikwad, F.M. Bellussi, S. Moitra, C.M. Megaridis, A new methodology for measuring solid/liquid interfacial energy, Journal of Colloid and Interface Science. 633 (2023) 800–807. https://doi.org/10.1016/j.jcis.2022.10.101.

[32] K. Onda, H. Takeuchi, Y. Okumoto, Mass Transfer Coefficients Between Gas and Liquid Phases in Packed Columns, Journal of Chemical Engineering of Japan. 1 (1968) 56–62. https://doi.org/10.1252/jcej.1.56.

[33] N. Ganan, J. Morchain, S. Camy, J.-S. Condoret, Rate-based simulation of a high pressure counter-current packed column for supercritical CO 2 extraction of alcohol from dilute aqueous mixtures, Journal of Supercritical Fluids. 135 (2018) 168–179. https://doi.org/10.1016/j.supflu.2018.01.020.

[34] A. Fabien, G. Lefebvre, B. Calvignac, P. Legout, E. Badens, C. Crampon, Interfacial tension of ethanol, water, and their mixtures in high pressure carbon dioxide: Measurements and modeling, Journal of Colloid and Interface Science. 613 (2022) 847–856. https://doi.org/10.1016/j.jcis.2022.01.058.

[35] National Institute of Standards and Technology, NIST. (n.d.). https://www.nist.gov/ (accessed February 9, 2022).

[36] D. Dittmar, S. Bijosono Oei, R. Eggers, Interfacial Tension and Density of Ethanol in Contact with Carbon Dioxide, Chemical Engineering & Technology. 25 (2002) 23–27. https://doi.org/10.1002/1521-4125(200201)25:1<23::AID-CEAT23>3.0.CO;2-8.

[37] * Andreas Hebach, and Alexander Oberhof, N. Dahmen, Density of Water + Carbon Dioxide at Elevated Pressures: Measurements and Correlation, (2004). https://doi.org/10.1021/je034260i.

[38] D. Pečar, V. Doleček, Volumetric properties of ethanol–water mixtures under high temperatures and pressures, Fluid Phase Equilibria. 230 (2005) 36–44. https://doi.org/10.1016/j.fluid.2004.11.019.

[39] G. Watson, C.K. Zéberg-Mikkelsen, A. Baylaucq, C. Boned, High-Pressure Density Measurements for the Binary System Ethanol + Heptane, J. Chem. Eng. Data. 51 (2006) 112–118. https://doi.org/10.1021/je050261u.

[40] L. Bernad, A. Keller, D. Barth, M. Perrut, Separation of ethanol from aqueous solutions by supercritical carbon dioxide — Comparison between simulations and experiments, The Journal of Supercritical Fluids. 6 (1993) 9–14. https://doi.org/10.1016/0896-8446(93)90004-H.

[41] J.S. Lim, Y.-W. Lee, J.-D. Kim, Y.Y. Lee, H.-S. Chun, Mass-transfer and hydraulic characteristics in spray and packed extraction columns for supercritical carbon dioxide-ethanol-water system, The Journal of Supercritical Fluids. 8 (1995) 127–137. https://doi.org/10.1016/0896-8446(95)90025-X.

[42] M. Budich, G. Brunner, Supercritical fluid extraction of ethanol from aqueous solutions, The Journal of Supercritical Fluids. 25 (2003) 45–55. https://doi.org/10.1016/S0896-8446(02)00091-8.

[43] C.A. Pieck, C. Crampon, F. Charton, E. Badens, Multi-scale experimental study and modeling of the supercritical fractionation process, The Journal of Supercritical Fluids. 105 (2015) 158–169. https://doi.org/10.1016/j.supflu.2015.01.021.

[44] F.J. Señoráns, A. Ruiz-Rodríguez, E. Ibañez, J. Tabera, G. Reglero, Countercurrent supercritical fluid extraction and fractionation of alcoholic beverages, J Agric Food Chem. 49 (2001) 1895–1899. https://doi.org/10.1021/jf001261v.

[45] F.J. Señoráns, A. Ruiz-Rodríguez, E. Ibañez, J. Tabera, G. Reglero, Optimization of countercurrent supercritical fluid extraction conditions for spirits fractionation, The Journal of Supercritical Fluids. 21 (2001) 41–49. https://doi.org/10.1016/S0896-8446(01)00086-9.

[46] F.J. Señoráns, A. Ruiz-Rodríguez, E. Ibáñez, J. Tabera, G. Reglero, Isolation of brandy aroma by countercurrent supercritical fluid extraction, The Journal of Supercritical Fluids. 26 (2003) 129–135. https://doi.org/10.1016/S0896-8446(02)00154-7.

[47] P. Legout, G. Lefebvre, M. Bonnin, J.-C. Gimel, L. Benyahia, O. Colombani, B. Calvignac, Synthesis of PDMS-b-POEGMA Diblock Copolymers and Their Application for the Thermoresponsive

Stabilization of Water-Supercritical Carbon Dioxide Emulsions, Langmuir. 36 (2020) 12922–12932. https://doi.org/10.1021/acs.langmuir.0c02194.

[48] A. Georgiadis, G. Maitland, J.P.M. Trusler, A. Bismarck, Interfacial Tension Measurements of the (H2O + CO2) System at Elevated Pressures and Temperatures, J. Chem. Eng. Data. 55 (2010) 4168–4175. https://doi.org/10.1021/je100198g.

[49] M. Brugnara, Contact Angle, (2006). https://imagej.nih.gov/ij/plugins/contact-angle.html (accessed April 16, 2022).

[50] P.J. Ramón-Torregrosa, M.A. Rodríguez-Valverde, A. Amirfazli, M.A. Cabrerizo-Vílchez, Factors affecting the measurement of roughness factor of surfaces and its implications for wetting studies, Colloids and Surfaces A: Physicochemical and Engineering Aspects. 323 (2008) 83–93. https://doi.org/10.1016/j.colsurfa.2007.10.032.

[51] Y. Sutjiadi-Sia, Interfacial Phenomena of Liquids in Contact with Dense CO_2, (2007). https://doi.org/10.15480/882.283.

[52] Y. Sutjiadi-Sia, P. Jaeger, R. Eggers, Interfacial tension of solid materials against dense carbon dioxide, Journal of Colloid and Interface Science. 320 (2008) 268–274. https://doi.org/10.1016/j.jcis.2007.12.021.

[53] A. Jarray, V. Magnanimo, S. Luding, Wet granular flow control through liquid induced cohesion, Powder Technology. 341 (2019) 126–139. https://doi.org/10.1016/j.powtec.2018.02.045.

[54] M. Tortora, S. Meloni, B.H. Tan, A. Giacomello, C.-D. Ohl, C.M. Casciola, The interplay among gas, liquid and solid interactions determines the stability of surface nanobubbles, Nanoscale. 12 (2020) 22698–22709. https://doi.org/10.1039/D0NR05859A.

[55] M. Décultot, A. Ledoux, M.-C. Fournier-Salaün, L. Estel, Solubility of CO2 in methanol, ethanol, 1,2-propanediol and glycerol from 283.15 K to 373.15 K and up to 6.0 MPa, The Journal of Chemical Thermodynamics. 138 (2019) 67–77. https://doi.org/10.1016/j.jct.2019.05.003.

[56] A. Marmur, Wetting on Hydrophobic Rough Surfaces: To Be Heterogeneous or Not To Be?, Langmuir. 19 (2003) 8343–8348. https://doi.org/10.1021/la0344682.

[57] N. Gao, Y. Yan, Modeling Superhydrophobic Contact Angles and Wetting Transition, Journal of Bionic Engineering. 6 (2009) 335–340. https://doi.org/10.1016/S1672-6529(08)60135-3.

[58] V. Hejazi, A.D. Moghadam, P. Rohatgi, M. Nosonovsky, Beyond Wenzel and Cassie–Baxter: Second-Order Effects on the Wetting of Rough Surfaces, Langmuir. 30 (2014) 9423–9429. https://doi.org/10.1021/la502143v.

[59] T. Onda, Theoretical Investigation of Wenzel and Cassie Wetting States on Porous Films and Fiber Meshes, Langmuir. 38 (2022) 13744–13752. https://doi.org/10.1021/acs.langmuir.2c01847.

[60] X. Wang, C. Fu, C. Zhang, Z. Qiu, B. Wang, A Comprehensive Review of Wetting Transition Mechanism on the Surfaces of Microstructures from Theory and Testing Methods, Materials. 15 (2022) 4747. https://doi.org/10.3390/ma15144747.

[61] J. Wang, H. Samara, V. Ko, D. Rodgers, D. Ryan, P. Jaeger, Analysis of the Impact of CO2 Adsorption on Rock Wettability for Geological Storage of CO2, Energy Fuels. (2023). https://doi.org/10.1021/acs.energyfuels.3c00909.

Figure captions

List of equations

Supporting Material

Appendix A

Pictures of apparent contact angles are presented for all studied conditions in the Figure 6.

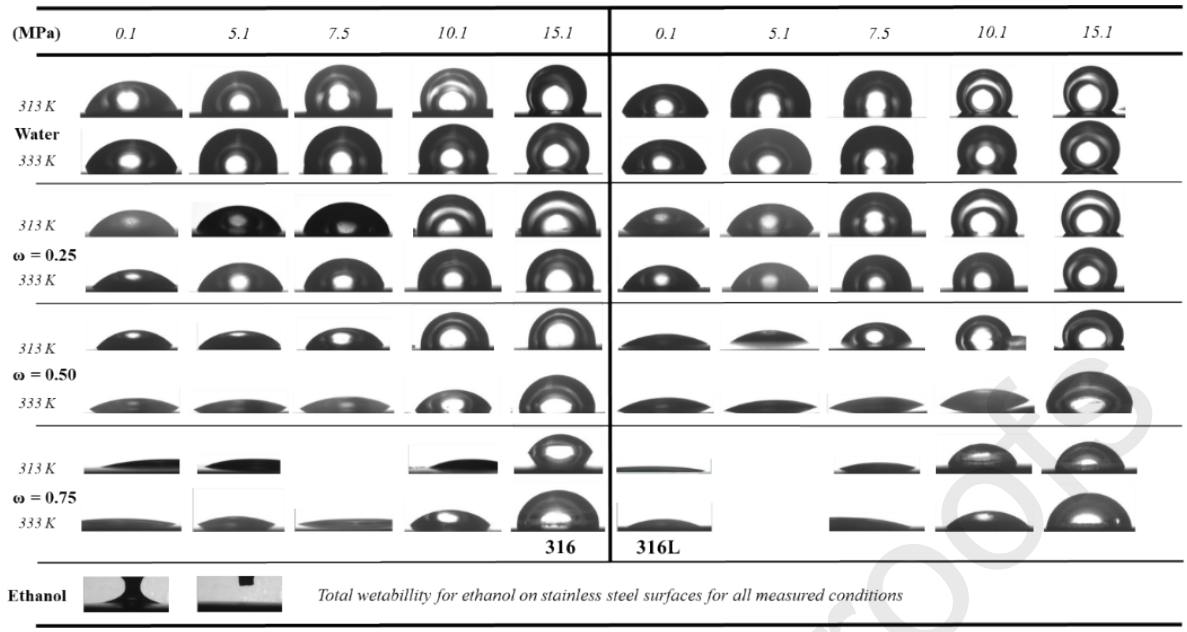

Figure 6 Apparent contact angles through all explored conditions

Appendix B

Corrections of the apparent contact angles through the Wenzel equation are presented for various roughness parameters in the Figure 7.

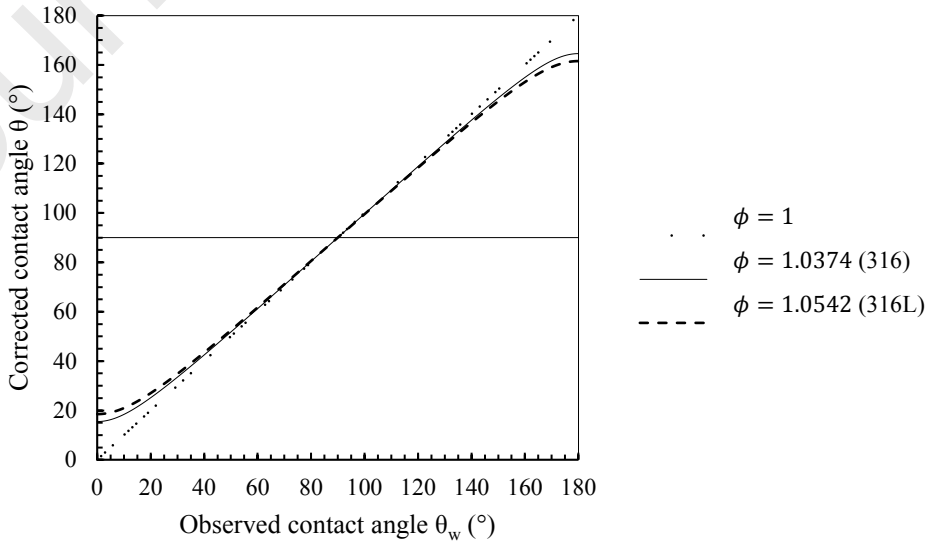

Figure 7 Roughness effect following the Wenzel equation considering maximal values of ϕ parameter for AISI 316 and AISI 316L surfaces

Appendix C

Table 1 and Table 2 regroup all averages of corrected contact angles obtained in this work with the statistical uncertainties calculated for a 95% confidence level. Each measurement was carried out at least in triplicate then corrected through the Wenzel equation and finally averaged.

Table 1 Data of corrected contact angle (CA) at 313.15 K for AISI 316 and AISI 316L with statistical uncertainties

P (MPa)	**T (K)**	**$\omega_{ethanol}$**	**CA 316 (°)**	**CA 316L (°)**
0.1	313.15	0	79 ± 8	78 ± 10
5.1	313.15	0	92 ± 4	103 ± 8
7.5	313.15	0	104 ± 6	108 ± 8
10.1	313.15	0	102 ± 6	122 ± 9

15.1	313.15	0	112	±	7	125	±	15
0.1	313.15	0.25	61	±	2	60	±	4
5.1	313.15	0.25	68	±	6	72	±	3
7.5	313.15	0.25	87	±	4	92	±	6
10.1	313.15	0.25	94	±	7	117	±	6
15.1	313.15	0.25	93	±	5	118	±	6
0.1	313.15	0.5	47	±	3	39	±	3
5.1	313.15	0.5	50	±	3	42	±	4
7.5	313.15	0.5	63	±	11	72	±	5
10.1	313.15	0.5	93	±	3	86	±	14
15.1	313.15	0.5	96	±	5	116	±	16
0.1	313.15	0.75	22	±	3	25	±	4
5.1	313.15	0.75	27	±	3			
7.5	313.15	0.75				27	±	3
10.1	313.15	0.75	33	±	4	64	±	9
15.1	313.15	0.75	62	±	3	82	±	6
0.1	313.15	1	0			0		
5.1	313.15	1	0			0		
7.5	313.15	1	0			0		

Table 2 Data of corrected contact angle (CA) at 333.15 K for AISI 316 and AISI 316L with statistical uncertainties

P (MPa)	T (K)	$\omega_{ethanol}$	CA 316 (°)	CA 316L (°)
0.1	333.15	0	66 ± 6	76 ± 1
5.1	333.15	0	97 ± 2	94 ± 3
7.5	333.15	0	96 ± 5	103 ± 3
10.1	333.15	0	102 ± 14	117 ± 2
15.1	333.15	0	117 ± 4	128 ± 3
0.1	333.15	0.25	51 ± 6	60 ± 7
5.1	333.15	0.25	56 ± 7	71 ± 4
7.5	333.15	0.25	77 ± 2	84 ± 4
10.1	333.15	0.25	94 ± 4	105 ± 5
15.1	333.15	0.25	105 ± 2	120 ± 1
0.1	333.15	0.5	38 ± 3	37 ± 3
5.1	333.15	0.5	34 ± 2	32 ± 4
7.5	333.15	0.5	34 ± 6	38 ± 6
10.1	333.15	0.5	63 ± 3	44 ± 5

15.1	333.15	0.5	82	±	3	78	±	3
0.1	333.15	0.75	21	±	1	27	±	4
5.1	333.15	0.75	24	±	5			
7.5	333.15	0.75	26	±	4	29	±	3
10.1	333.15	0.75	53	±	5	47	±	2
15.1	333.15	0.75	75	±	3	77	±	4
0.1	333.15	1	0			0		
5.1	333.15	1	0			0		
7.5	333.15	1	0			0		
10.1	333.15	1	0			0		

Appendix D

The ratio γ_{SF}/γ_{LF} of water at 313 K in saturated dense CO_2 as a function of pressure is presented in Figure 8. Data of γ_{SF} are taken from [52] and data of γ_{LF} are taken from [34].

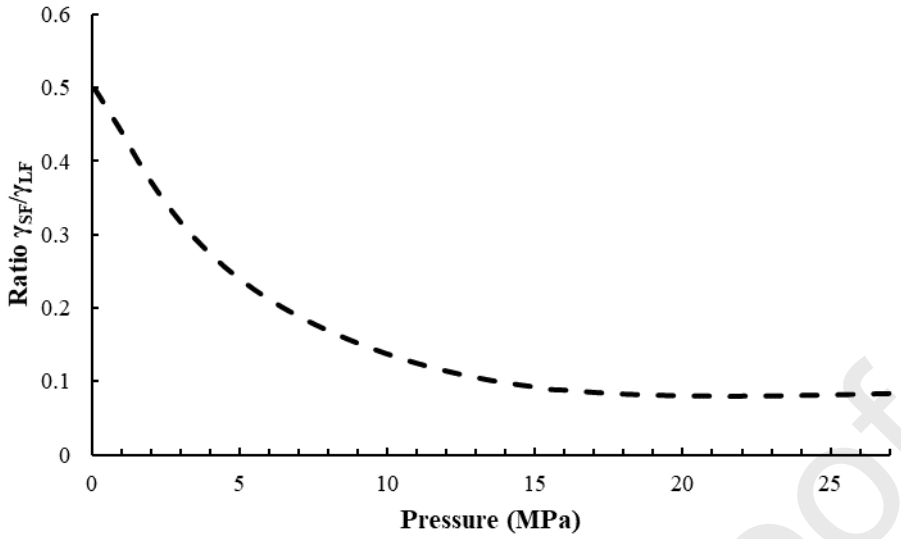

Figure 8 Ratio γ_{SF}/γ_{LF} as a function of pressure for CO_2/water/ stainless steel system at 313 K, data used are from [52] for γ_{SF} and from *[34] for γ_{LF}*

Appendix E

Influence of the chemical heterogeneity of the solid/liquid interface for various arbitrary wetted fraction σ is presented in Figure 9.

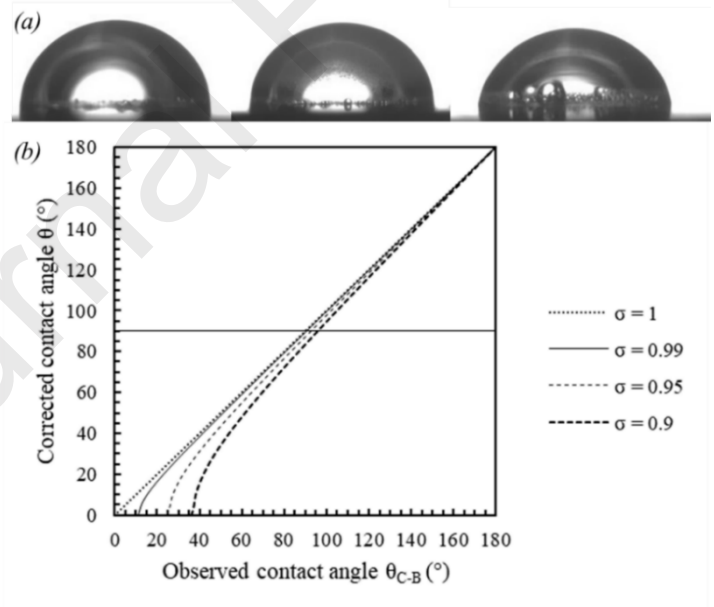

Figure 9 (a) picture of trapped bubbles, (b) correction of the observed contact angle through the Cassie-Baxter equation for various arbitrary wetted fraction

Graphical abstract

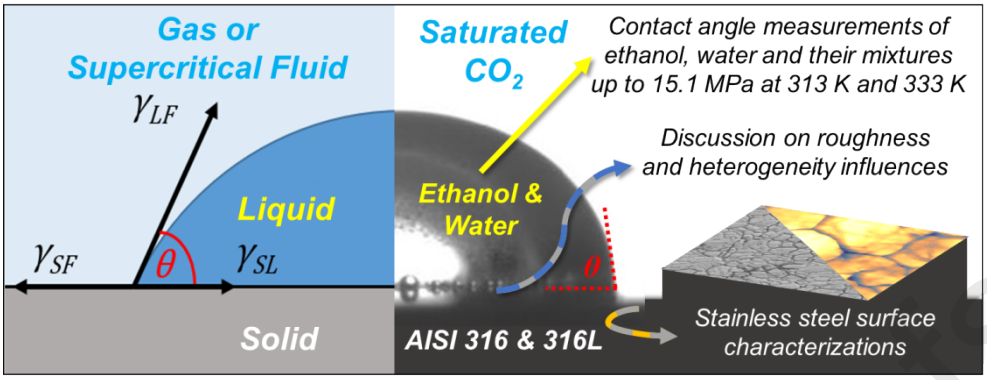

Credit Author Statement

Aymeric Fabien: Conceptualization, Methodology, Investigation, Validation, Formal analysis, Writing - Original Draft, Writing - Review & Editing, Visualization

Guillaume Lefebvre: Conceptualization, Methodology, Resources, Investigation, Validation, Writing - Review & Editing, Supervision

Elisabeth Badens: Conceptualization, Methodology, Resources, Writing - Review & Editing, Supervision, Project administration, Funding acquisition

Brice Calvignac: Conceptualization, Methodology, Resources, Writing - Review & Editing, Supervision

Damien Chaudanson: (SEM-FEG analysis) Resources, Investigation, Validation, Formal analysis

Alain Ranguis: (AFM analysis) Resources, Investigation, Validation, Formal analysis

Christelle Crampon: Conceptualization, Methodology, Resources, Writing - Review & Editing, Supervision, Project administration, Funding acquisition

Declaration of interests

☒ The authors declare that they have no known competing financial interests or personal relationships that could have appeared to influence the work reported in this paper.

☐The authors declare the following financial interests/personal relationships which may be considered as potential competing interests: